PCCP

Accepted Manuscript

ROYAL SOCIETY OF CHEMISTRY

www.rsc.org/pccp

Journal Name

ARTICLE

Origins of Ultralow Thermal Conductivity in Bulk [6,6]-Phenyl-C_{61}-Butyric Acid Methyl Ester (PCBM)

Received 00th January 20xx,
Accepted 00th January 20xx

DOI: 10.1039/x0xx00000x

www.rsc.org/

Jan-Hendrik Pöhls[a], Michel B. Johnson[b,c], and Mary Anne White[*a,b,c]

Bulk PCBM has exceptionally low thermal conductivity, 0.07 W m^{-1} K^{-1} at room temperature. We show that its ultralow thermal conductivity is an intrinsic property. Based on results for thermal conductivity and heat capacity measurements down to < 2 K, along with Raman spectroscopy and dilatometry, a new model for minimum thermal conductivity was developed. In the model the thermal energy is transferred between entities of phonons oscillating in a range of frequencies, and limited by the atomic density and the phonon mean speed. The model accurately represents the low thermal conductivity for both PCBM and C_{60}/C_{70}.

Introduction

PCBM ([6,6]-phenyl-C_{61} butyric acid methyl ester) is a commonly used fullerene derivative with wide applications in organic electronics, such as the electron acceptor in bulk hetero-junction (BHJ) solar cells [1]. Organic electronics containing PCBM are well known, but surprisingly the properties of pure PCBM are not, which is especially unusual considering that the parent compound, fullerene, is a widely studied material with unique properties [2,3].

Recent studies by Duda *et al.* showed that thin films of PCBM have the lowest reported room-temperature thermal conductivity for a fully dense solid: κ = 0.030 ± 0.003 W m^{-1} K^{-1} [4], as verified by Wang *et al.* [5] and Guo *et al*. [6] but with slightly higher values (κ = 0.057±0.007 and 0.07±0.007 W m^{-1} K^{-1}, respectively). Recent molecular dynamic (MD) simulations computed the phonon dispersion of PCBM and predicted that its thermal conductivity is in the range 0.05 to 0.075 W m^{-1} K^{-1} [7].

The useful concept of a lower theoretical limit of the thermal conductivity was introduced by Cahill *et al.* [8]. However, several materials, including WSe_2 [9], CdSe [10], and SnSe [11], have been found to have thermal conductivities lower than the theoretical minimum; these are known as ultralow thermal conductivity materials. For PCBM a theoretical minimum thermal conductivity of ~ 0.3 W m^{-1} K^{-1} was calculated using the Cahill-Pohl model [8] with the speed of sound [4], and it is much higher than the reported experimental thermal conductivity. Therefore, the thermal conductivity is considered to be ultralow. However, thin films can have lower thermal conductivities than their corresponding bulk materials [12,13] so it was not clear if the low value was intrinsic to PCBM or due to morphology.

In this report we present the bulk thermal conductivity of PCBM and show that the ultralow thermal conductivity of PCBM is an intrinsic property. Furthermore, we delineate the origins of the ultralow thermal conductivity in PCBM via heat capacity measurements.

Materials and methods

PCBM powder (>99%; Solenne BV, Netherlands) was used as received. To prepare pellets for thermal measurements, PCBM powder was placed in a stainless steel die (diameter = 5.08 mm) and consolidated with a pressure of 440 MPa for 15 min in air. Powder X-ray diffraction (PXRD) data were collected, both before and after consolidation, on a zero-background holder using a Rigaku Ultima IV PXRD with a monochromatic CuKα beam (λ = 1.540 Å), a graphite monochromator, and a Ni filter. For the temperature-dependent PXRD a Siemens D500 with a temperature stage was used.

The thermal conductance of a consolidated PCBM pellet (diameter = 5.08 ± 0.02 mm, thickness = 0.90 ± 0.02 mm, and mass density = 1.52 ± 0.02 g cm^{-3}) was measured in steady-state conditions from 2 K to 398 K using a Physical Property Measurement System (PPMS, from Quantum Design). The pellet was adhered between two gold-plated copper disks using silver-loaded epoxy (Tra-Bond 2902) and affixed to the thermal transport stage. The thermal conductivity was determined from the measured thermal conductance and the geometry of the PCBM pellet. Blackbody radiation was

a Department of Physics, Dalhousie University, Halifax, NS B3H 4R2, Canada
b Institute for Research in Materials, Dalhousie University, Halifax, NS B3H 4R2, Canada
c Department of Chemistry, Dalhousie University, Halifax, NS B3H 4R2, Canada
* Corresponding author: Mary Anne White, mary.anne.white@dal.ca†

corrected using a sample emissivity of one. Further details about the thermal transport technique are given elsewhere [14,15].

Heat capacity was determined from 0.4 K to 300 K by thermal-relaxation micro-calorimetry with a PPMS under high vacuum (<10^{-4} Torr). The relaxation calorimetry technique for both ^{4}He and ^{3}He cooling is described in detail elsewhere [16].

Raman spectra were recorded from 50 cm^{-1} to 1800 cm^{-1} with a Nicolet NXR 9650 FT-Raman spectrometer (Thermo Fisher Scientific) equipped with a 1064 nm Nd:YVO_4 laser. The laser power and resolution were set to 0.04 W and 2 cm^{-1}, respectively.

The thermal expansion properties of two consolidated PCBM pellets (thickness = 1.194 ± 0.003 mm and 1.213 ± 0.002 mm) were determined with a Netzsch Dilatometer DIL 402C. The dilatometer was calibrated with a quartz sample and heated at a rate of 10 K min^{-1} from room temperature to 220 °C, and cooled to room temperature in air.

Differential scanning calorimetry (DSC, Q200 from TA Instruments™) was used to determine potential phase transitions. Thermograms of PCBM powder (m = 3.47 mg) and pellet (m = 4.85 mg) were recorded with a scanning rate of 10 K min^{-1} under He atmosphere. For thermogravimetric analysis studies a SDT Q600 thermogravimetric analyzer (TGA) from TA Instruments™ was used with a scanning rate of 10 K min^{-1} in air.

Results and discussion

Ultralow thermal conductivity from direct measurement for a solvent-free consolidated PCBM pellet [17], corrected to zero porosity [18] was determined as a function of temperature (Figure 1). The present room-temperature data are in the range of the computed thermal conductivity [7] and within the uncertainty of solvent-free PCBM thin films in two previous reports [5, 6], but more than twice the value from Duda *et al.* [4].

We characterized the bulk PCBM sample thoroughly to allay concerns about changes associated with pressing pellets. The powder x-ray diffraction (PXRD) pattern of the as-received PCBM powder and the consolidated pellet showed no significant change in crystal structure (Fig. S1 in the Supplemental Materials [17]). The pellets had only a small decrease in unit cell volume after pressing (V_{powder} ~ 3761 Å^3, and V_{pellet} ~ 3752 Å^3; Table S1 [17]), slightly different from the solvent-free PCBM thin films ($V_{thinfilm}$ = 3733 Å^3) [11]. Corroborating the PXRD findings, no significant difference in the Raman spectra of PCBM powder and pellet was observed (Fig. 2 (a) and (b)), indicating an intact molecular structure after pressing. (The assignment of the Raman modes is discussed in the Supplemental Materials [17].) Therefore, the ultralow thermal conductivity of PCBM is not influenced by consolidation.

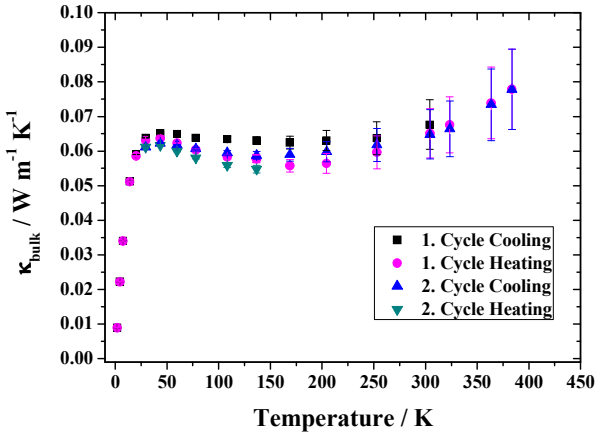

FIG. 1: Thermal conductivity of bulk PCBM pellet showing only a small hysteresis for two cooling/heating cycles. The increase in κ for T > 300 K might be due to black-body radiation.

One more factor to consider is that in low thermal conductivity materials non-steady state conditions could dramatically influence the thermal conductivity determination. Due to its ultralow thermal conductivity, thermal gradients in a PCBM pellet require a long time to reach steady state, and in separate experiments in which steady state was not fully achieved, we found that the thermal conductivity was artificially low by about a factor of 3. However, for the results reported, steady-state conditions were achieved, as evidenced by the observation of only a small hysteresis for different thermal conductivity cycles (Fig. 1).

In contrast to the present steady-state thermal transport direct determination of thermal conductivity, the thermal conductivity in PCBM thin films was determined by time domain thermoreflectance (TDTR) [4,5,6] and further parameters such as the specific heat are needed to determine κ. Here we directly determined the specific heat of PCBM as a function of temperature (Fig. 3 (a); data in Tables S6-S9 [17]). Although the specific heat data here have a larger than ideal [12] uncertainty due to low thermal conductivity (uncertainty < 7% from 300 K to 5 K, < 15% from 5 K to 0.4 K), we have reasonable accuracy for the room-temperature specific heat, 0.82±0.02 J g^{-1} K^{-1}, based on four PCBM pellets with different masses. This value is close to the specific heat of 0.68 J g^{-1} K^{-1} determined by Wang *et al.* for evaporated PCBM thin films [5]. Therefore the factor of ~2 difference in thermal conductivity between the results from Duda *et al.* [4] and our results (which coincide with the other earlier studies [5,6]), is not likely due to the heat capacity used to convert TDTR results to thermal conductivity.

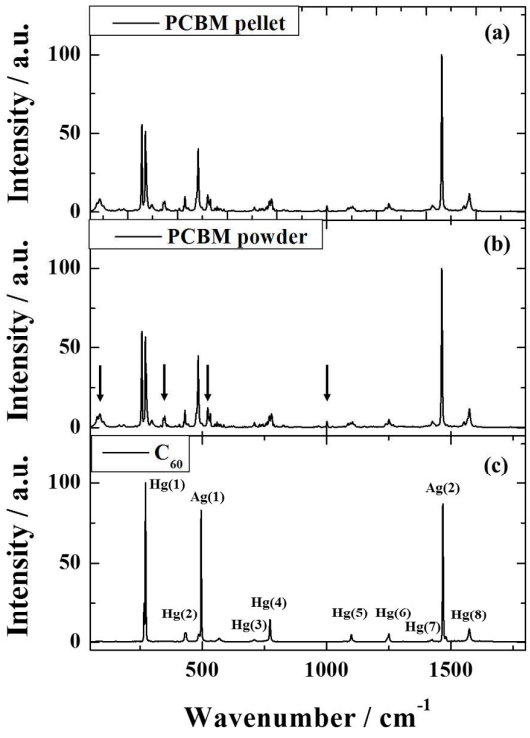

FIG. 2: Experimentally determined Raman spectra of (a) PCBM pellet, (b) PCBM powder, and (c) C_{60} powder. While no significant discrepancy between PCBM powder and PCBM pellet spectra was recorded, the number of modes increased from C_{60} to PCBM due to the reduction in symmetry. See Supplementary Material [17] for discussion of the spectra.

However, an unknown factor is the porosity of the thin films. While we adjusted the thermal conductivity of the pellets to zero porosity (which raised the thermal conductivity by ~9%), the porosity of the PCBM thin films measured in the earlier TDTR experiments was not reported.

Further consideration of the specific heat itself is revealing. As shown in Fig. 3 (b), the thermal evolution of specific heats is similar for C_{60}/C_{70} [19], C_{60} [20] and PCBM. A similar temperature dependence also was found for the thermal conductivity of PCBM (Fig. 1) and C_{60}/C_{70} fullerite [19] (Fig. S2 [17]), showing a strong correlation between the heat capacity and the ultralow thermal conductivity in PCBM and C_{60}/C_{70}. To understand the origins of the ultralow thermal conductivity in PCBM, its heat capacity is considered further.

The C_p/T^3 values averaged for four PCBM pellets show (Fig. 3 (c)) a broad peak at T = 4.5 K suggesting the presence of low-frequency optical modes [15] or two-level states (TLS) where atoms can occupy two or more potential wells [21,22,23]. Although the broad peak looks similar to a peak found for TLS in glassy and highly-disordered materials at low temperatures, there is no evidence of TLS in PCBM. For systems with TLS, the heat capacity (C/T^3) typically has a peak above 10 K and the thermal conductivity increases with a T^2 behavior to a plateau at ~10 K [21]. In PCBM, the peak heat capacity peak appears at 4.5 K and the thermal conductivity increases with $T^{0.8}$ behavior to a plateau at ~30 K.

It is more likely that the low temperature peak appears due to low-frequency optical modes; a similar peak [24] as well as low-frequency optical modes were found in the parent compound C_{60} [25,26]]. Beyermann *et al.* showed that the low-temperature heat capacity of C_{60} can be fit by the sum of two Debye terms, two Einstein terms, and a linear term [24]. Here the acoustic modes of PCBM were modeled with one Debye term with a total number of Debye oscillators per unit cell of n_D = 0.25 because it is assumed that the rotation of the molecules is hindered by the side chains [24]. Our best fit was achieved with four different Einstein terms (n_{E1} = 0.083, θ_{E1} = 15 K; n_{E2} = 0.58, θ_{E2} = 26 K; n_{E3} = 0.33, θ_{E3} = 48 K; n_{E4} = 1.00, θ_{E4} = 55 K), where n_E is the number of Einstein oscillators per unit cell and θ_E is the Einstein temperature (Fig. 3 (c)). The first two Einstein terms most likely correspond to librational modes in which rigid PCBM molecules 'rock' at their equilibrium positions. Horoyski *et al.* reported two slightly higher librational modes for C_{60} (θ_E = 25.3 K and θ_E = 30.2 K) using Raman spectroscopy at 85 K [25], similar to the report of Bagatskii *et al*. of a libration Einstein temperature of 32.5 K [26]. Horoyski *et al.* also found that the energy of the librational modes increases with increasing pressure and decreasing temperature, due to contraction of the unit cell [25]. PCBM molecules are less densely packed than C_{60} (ρ_{PCBM}= 1.613 g cm^{-3}, ρ_{C60} = 1.678 g cm^{-3} [27]) which could result in lower intermolecular interaction energies and therefore lower frequencies. In addition to the low-frequency librational modes in PCBM, two other Einstein terms have higher frequencies (θ_{E3} = 48 K and θ_{E4} = 55 K). This analysis leads to a total of three librational modes per PCBM molecule. The higher-frequency modes are comparable to the Einstein modes found by Beyermann *et al.* for C_{60} (θ_E = 58 K) [24] and are in the range of intermolecular translational modes [28].

An anomaly in the heat capacity of PCBM expressed as C_p/T was detected at T ~ 90 K (Fig. 3 (d)), as also observed for C_{60} and C_{60}/C_{70} [19,20,]. The lower-temperature peak in C_p/T^3 from T ~1.6 K to 90 K is fit well by the parameters in Fig. 3 (c). However, three additional optical modes in PCBM as observed by Raman spectroscopy (Fig. 2), contribute significantly to the heat capacity from ~30 K to ~200 K. These optical modes are most likely associated with vibrations of the side chain, and result in an increase of the heat capacity of PCBM relative to C_{60} [20] (Fig. 3 (b)). The large increase in C_p/T at higher temperatures occurs due to the excitation of intramolecular modes. In particular, the A_g breathing mode for the C_{60} moiety of PCBM has a large contribution to the increase in C_p/T as illustrated in Fig. 3 (d). Note that assignments of silent modes (32 for C_{60} [29]) and IR modes of PCBM molecules were not considered for the fit and therefore the contribution for each mode is not representative of exact lattice dynamics. Although this analysis of the vibrational modes in PCBM is only semi-quantitative, it indicates a large separation between the

frequencies of intermolecular and intramolecular modes, as also found in C_{60} [29].

In addition to the optical modes, the Debye temperature determined from the fit (θ_D = 37 K) and the slope of the linear C_p term (a = 0.72 mJ mol^{-1} K^{-2}) are both lower than for C_{60} (θ_{D1} = 49 K, θ_{D2} = 67 K, a = 45 mJ mol^{-1} K^{-2} [24]). The low Debye temperature in PCBM is most likely due to lower interaction energies between the PCBM molecules than in C_{60} resulting in a softer PCBM lattice, as also was seen from the speed of sound [4]. The a value for PCBM is correspondingly low, However, a hexagonal unit cell with one PCBM molecule was used for the MD simulation which is not consistent with our PXRD result (Fig. S1 and Table S1 [17]). At higher temperature (T > 20 K) the calculated heat capacity is very close to the experimental results.

To compare the heat capacities of C_{60}/C_{70} [19] and PCBM, the low-temperature heat capacity of C_{60}/C_{70} fullerite was fit with the same approach as for PCBM (see Supplemental Materials [17]). While the Einstein terms are almost the same, the Debye temperature increased for C_{60}/C_{70} to θ_D = 54 K. The

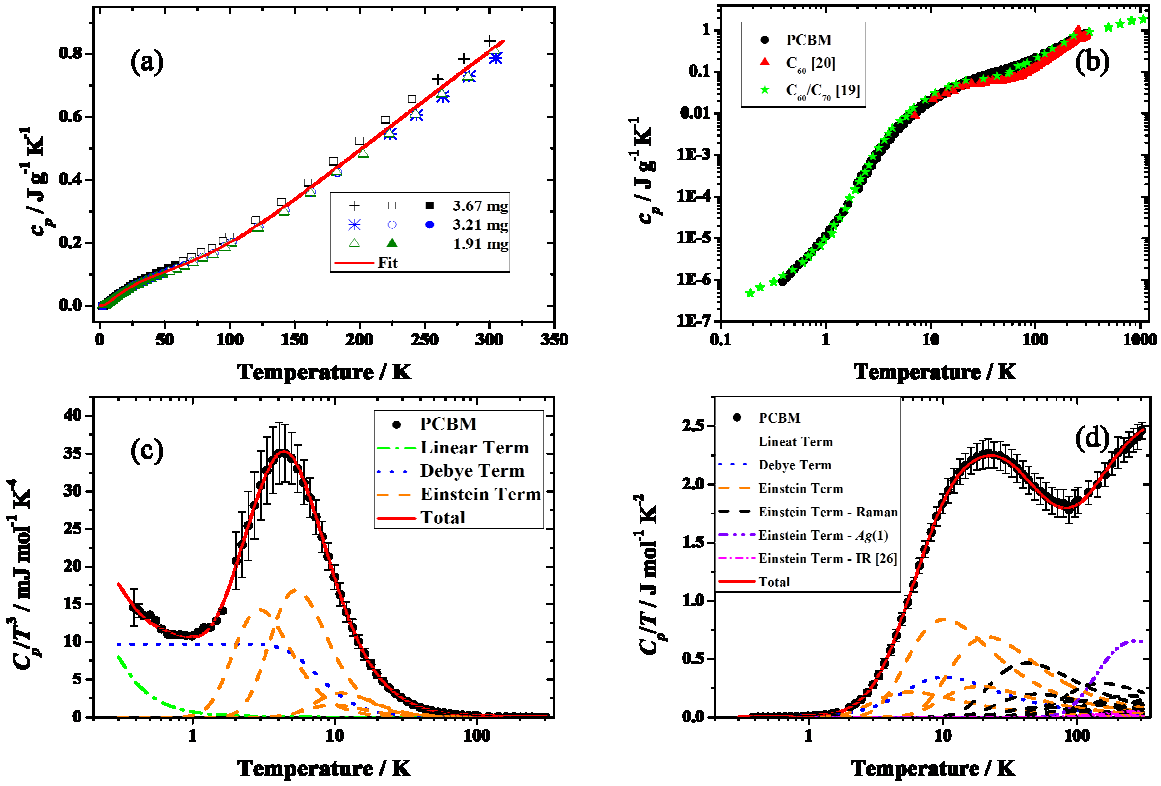

FIG. 3: (a) Specific heat of several different PCBM pellets, each with a different symbol, with masses as indicated [17]; red curve is the fit (see (d)). (b) Specific heat of PCBM showing a shape similar to C_{60} [20] and C_{60}/C_{70} fullerite [19]. (c) C_p/T^3 vs T of PCBM fit with one Debye term, four Einstein terms, and one linear term. (d) C_p/T vs T fit as in (c) with additional Einstein terms from Raman experiments and IR data [29]. For the heat capacity curves in (c) and (d) the average C_p values for four PCBM pellets were used and the uncertainty shown is their standard deviation.

in the range of glassy materials [30] and about 1/3 the value for C_{60}/C_{70} fullerite [19]. The Debye temperature and heat capacity were also compared to the calculated heat capacity of PCBM using the phonon density of states of MD simulations [7] and a canonical partition function [31]. Although a higher heat capacity at low temperature was calculated than observed, the computed Debye temperature was almost a factor of three higher (θ_D = 99 K). The high heat capacity at low temperature is a result of a contribution of low-frequency optical modes. difference in thermal conductivity, therefore, cannot be explained by the Einstein model of minimum thermal conductivity which uses only the optical modes [32]. Based on this model, Cahill *et al.* developed an approach to calculate the lower limit of the thermal conductivity in disordered crystals [8]. Whereas Einstein assumed that the thermal energy is transported between neighboring atoms vibrating with a single frequency, Cahill *et al.* proposed that the energy is transferred between collective vibrations of atoms over a range of

frequencies [8]. The Cahill-Pohl model of minimum thermal conductivity provides an overestimate by a factor of ~5 for PCBM [4]. Therefore, we modified the Cahill-Pohl model to describe the lowest limit of thermal conductivity in any bulk solid.

For the derivation of the modified minimum thermal conductivity, κ_{min}, we start with the same approach as Cahill *et al.* [33]

$$\kappa_{min} = \sum_i \int_0^{\omega_D} \frac{1}{3} D_i(\omega) C_V(\omega) \bar{v}_i \lambda \, \mathrm{d}\omega \qquad (1)$$

where ω_D is the Debye frequency, $D_i(\omega) = V \frac{\omega^2}{2\pi^2 v_g v_p{}^2}$ is the volumetric density of states, $C_V(\omega)$ is the heat capacity per unit volume, $\bar{v}_i$ is the phonon mean speed, and λ is the phonon mean free path. The first new concept concerns the fact that the speed of sound is higher than the actual mean speed of the phonons in the material and therefore speeds of sound from ultrasound measurements would overestimate the minimum thermal conductivity. Whereas Debye assumed a linear dispersion in the first Brillouin zone with a constant velocity, in real crystals the dispersion is not linear, as indicated by Born and von Kármán [34] (see Fig. S2 (a) [17]). If the frequency is in the range of ultrasound measurements (MHz to GHz), the speed is constant and defined as the speed of sound, v_s. At higher frequencies, the dispersion is non-linear and therefore the phase velocity, $v_p = \frac{\omega}{k}$, and the phonon group velocity, $v_g = \frac{\partial \omega}{\partial k}$, have to be considered for the calculation of the volumetric density of states (Fig. S2 (a) [17]). If the averages of the frequency-dependent phase velocity and group velocity, $\langle v_p \rangle$ and $\langle v_g \rangle$, are taken, we get a constant phonon mean speed

$$\bar{v} = \left(\langle v_g \rangle \langle v_p \rangle^2 \right)^{1/3} = \frac{k_B \theta_D}{\hbar} \left(\frac{V}{6\pi^2 N} \right)^{1/3} \qquad (2)$$

and thus, $D(\omega) = V \frac{\omega^2}{2\pi^2 \bar{v}^3}$. As shown in Fig. S2 (a) [17], the mean phonon speed in the Debye model is lower than the speed of sound in the Born-von Kármán model [17]. In particular, for low thermal conductivities, we now assume that the dispersion is curved and only small wavelengths contribute to the thermal conductivity, resulting in a larger difference between speed of sound and phonon mean speed. Morelli *et al.* compared the Debye temperature from ultrasound measurements and specific heat; they found a reduction in the Debye temperature if determined from specific heat [35]. It is important to note that the derivation of the minimum thermal conductivity and the Debye heat capacity ($C_{Debye} = \frac{\mathrm{d} \int_0^{\omega_D} D(\omega) \langle E \rangle \mathrm{d}\omega}{\mathrm{d}T}$ where $\langle E \rangle$ is the average energy [36]) are both functions of the volumetric density of states. Therefore, the Debye temperature, θ_D, from the heat capacity measurements can be used to calculate a new lower limit of the thermal conductivity.

Our second modification to the Cahill-Pohl model of minimum thermal conductivity was the application of a constant phonon mean free path $\left(\lambda = \left[\frac{\pi V}{6N} \right]^{1/3} \right)$, in place of a frequency-dependent phonon mean free path ($\lambda_i = \frac{\pi}{\omega_i} \bar{v}_i$) [8]. If the phonon mean free path was frequency-dependent, the phonon mean free path would approach infinity for low frequencies. This contradicts the grain boundary limit which is frequency-independent and proportional to the grain size [37]. Therefore, we assume for the true minimum thermal conductivity that even low-frequency modes are limited by the atomic distribution in the unit cell. A similar assumption was made by Feser *et al.* where the mean free path is limited by the grain boundary [10]. It is important to note that similar to

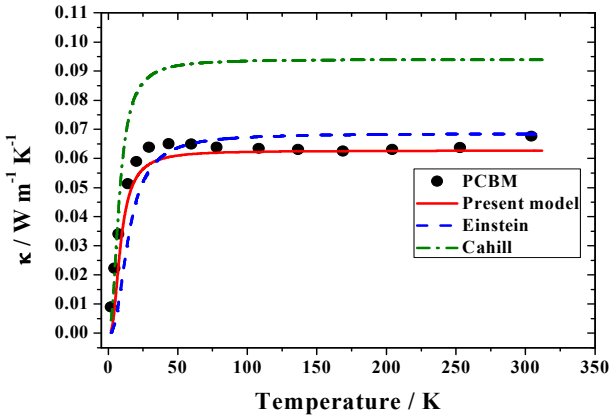

FIG. 4: Thermal conductivity of PCBM fitted with different models for minimum thermal conductivity. The present model agrees well with the experimental thermal conductivity for PCBM.

using the average grain size for the scattering event of grain boundaries, the atomic density can be applied as an average of the bond lengths although the atomic distances vary in and between the PCBM molecule(s).

Using these two new concepts and the heat capacity per unit volume taken from Einstein $\left(C_V = \frac{k_B}{V} \frac{x^2 e^x}{e^x - 1} \right)$ [32] with $x = \frac{\hbar \omega}{k_B T}$ (k_B is the Boltzmann constant and h is Planck's constant) the lowest thermal conductivity is then defined as

$$\kappa_{min} = \frac{3}{6^{2/3} \pi^{1/3}} \frac{k_B^2}{\hbar} \left(\frac{N}{V} \right)^{1/3} \frac{\theta_D}{x_D{}^3} \int_0^{x_D} \frac{x^4 e^x}{(e^x - 1)^2} \mathrm{d}x, \qquad (3)$$

with $x_D = \frac{\theta_D}{T}$ and N/V = 9.38·10^{22} cm^{-3} and θ_D = 37 K from our heat capacity fit. The κ_{min} values calculated with the present model accurately represent the experimental data (Fig. 4). It is important to note that the Debye temperature and the Einstein temperatures from the heat capacity fits were used for the calculation of the minimum thermal conductivity of the Cahill-Pohl model and the Einstein model, respectively; otherwise, the discrepancy between those models and the experimental result would be even larger.

The above analysis is independent of thermal expansion, but based on equation (3), the thermal conductivity should decrease with increasing unit cell volume. We determined the thermal expansion of a PCBM by dilatometry (Fig. S3 [17]) and PXRD (Fig. S4 [17]). From 123 K to 223 K, the volume increased and then was almost constant from 223 K to 373 K [17]. A decrease in thermal conductivity was observed between 40 K

and 150 K (Fig. 1), consistent with thermal expansion at low temperature. The nearly constant unit cell volume between 223 K and 373 K is consistent with Raman spectra where no peak shift was observed over that temperature range (see Fig. S5). At higher temperature (T > 450 K), irreversible expansion was observed by dilatometry (Fig. S3 [17]), consistent with the PXRD at 473 K which showed a change in structure (Fig. S4 [17]). High-temperature behavior, including phase transformations, is discussed further in the Supplemental Materials [17].

Conclusions

Bulk PCBM has the lowest thermal conductivity reported for a fully dense bulk material. We introduce a new minimum thermal conductivity model where the thermal energy is transferred between entities of phonons oscillating in a range of frequencies. We assumed that the energy transfer is limited by the atomic density and the phonon mean speed, with the latter determined from the experimental Debye temperature. The present model agrees with the data for both PCBM (Fig. 4) and C_{60}/C_{70} (see Fig. S2 (d) [17]). This model might be useful to describe other ultralow thermal conductivity materials. The optical phonons of PCBM do not contribute directly to the thermal conductivity, which then leads to a nearly temperature-independent thermal conductivity over a wide temperature range, as observed experimentally. From the heat capacity results, the breathing mode of the fullerene core has a large contribution to the heat capacity, and a distinct separation between intra- and intermolecular phonons was observed. The change from intramolecular mode to intermolecular modes is not as distinct as in C_{60} [20] due to low-frequency intermolecular modes; these modes were also observed by Raman spectroscopy.

Acknowledgements

J-H.P. acknowledges support from Dalhousie Research in Energy, Advanced Materials and Sustainability (DREAMS), an NSERC CREATE program. We acknowledge support from NSERC, the Canada Foundation for Innovation, and Atlantic Innovation Fund and other partners that fund the Facilities for Materials Characterization managed by the Institute for Research in Materials at Dalhousie University. We appreciate the assistance of S. Corbin (dilatometry), J. Dahn (TGA), A. George and M. Obrovac (PXRD). Furthermore, we appreciate useful discussions with E. Johnson, J. Zwanziger, L. Chen, X. Wang, and S. Kumar.

References

1. M. A. Brady, G. M. Su, and M. L. Chabinyc, *Soft Matter*, 2011, **7,** 11065.
2. V. Blank, M. Popov, G. Pivovarov, N. Lvova, K. Gogolinsky, and V. Reshetov, *Diamond Relat. Mater.*, 1998, **7,** 427.
3. T.L. Makarova, B. Sundqvist, R. Höhne, P. Esquinazi, Y. Kopelevich, P. Scharff, V.A. Davydov, L.S. Kashevarova, and A.V. Rakhmaninova, *Nature*, 2001, **413**, 716.
4. J. C. Duda, P. E. Hopkins, Y. Shen, and M. C. Gupta, *Phys. Rev. Lett.*, 2013, **110,** 015902.
5. X. Wang, C. D. Liman, N. D. Treat, M. L. Cabinyc, and D. G. Cahill, *Phys. Rev. B*, 2013, **88,** 075310.
6. Z. Guo, D. Lee, J. Strzalka, H. Gao, L. Huang, A. M. Khounsary, and T. Luo. *Phys. Chem. Chem. Phys.*, 2014, **16**, 26359.
7. L. Chen, X. Wang, and S. Kumar, *Sci. Rep.*, 2015, **5**, 12763.
8. D. G. Cahill, S. K. Watson, and R. O. Pohl, *Phys. Rev. B*, 1992, **46**, 6131.
9. C. Chiritescu, D. G. Cahill, N. Nguyen, D. Johnson, A. Bodapati, P. Keblinski, and P. Zschak, *Science*, 2007, **315**, 351.
10. J. P. Feser, E. M. Chan, A. Majumdar, R. A. Segalman, and J. J. Urban, *Nano Lett.*, 2013, **13**, 2122.
11. L.-D. Zhao, S.-H. Lo, Y. Zhang, H. Sun, G. Tan, C. Uher, C. Wolverton, V. P Dravid, and M. G. Kanatzidis, *Nature*, 2014, **508**, 373.
12. M. Asheghi, Y. K. Leung, S. S. Wong, and K. E. Goodson, *Appl. Phys. Lett.*, 1997, **71,** 1798.
13. Z. Yan, C. Jiang, T. R. Pope, C. F. Tsang, J. L. Stickney, P. Goli, J. Renteria, T. T. Salguero, and A. A. Baldanin, *J. Appl. Phys.*, 2013, **114,** 204301.
14. O. Maldonado, *Cryogenics*, 1992, **32,** 908.
15. C. A. Kennedy and M. A. White, *Solid State Commu.*, 2005, **134,** 271.
16. C. A. Kennedy, M. Stancescu, R. A. Marriott and M. A. White, *Cryogenics* **47**, 107-112 (2007).
17. See Supplemental Materials at [journal to insert url] for details.
18. P. G. Klemens, *High Temp. – High Pressures*, 1991, **23,** 241.
19. J. R. Olson, K. A. Topp, and R. O. Pohl. *Science*, 1993, **259,** 1145.
20. T. Matsuo, H. Suga, W. I. F. David, R. M. Ibberson, P. Bernier, A. Zahab, C. Fabre, A. Rassat, and A. Dworkin, *Solid State Commu.*, 1992, **83**, 711.
21. Y. M. Galperin, V. G. Karpov, and V. I. Kozub, *Adv. Phys.*, 1989, **38**, 669.
22. W. A. Phillips, *Rep. Prog. Phys.*, 1987, **50**, 1657.
23. B. Rufflé, D. A. Parshin, E. Courtens, and R. Vacher, *Phys. Rev. Lett.*, 2008, **100**, 015501.
24. W. P. Beyermann, M. F. Hundley, J. D. Thompson, F. N. Diederich, and G. Grüner, *Phys. Rev. Lett.*, 1992, **68,** 2046.
25. P. J. Horoyski, J. A. Walk, and M. L. W. Thewalt, *Solid State Commu.*, 1995, **93,** 575.
26. M. I. Bagatskii, V. V. Sumarokov, M. S. Barabashko, A. V. Dolbin, and B. Sundqvist, *Low Temp. Phys.*, 2015, **41**, 630.
27. D. A. Neumann, J. R. D. Copley, W. A. Kamitakahara, J. J. Rush, R. L. Cappelletti, N. Coustel, J. E. Fischer, J. P. McCauley, A. B. Smith, K. M. Creegan, and D. M. Cox. J, *Chem. Phys.*, 1992, **96**, 8631.
28. W. Krätschmer, L. D. Lamb, K. Fostirpoulos, and D. R. Huffman, *Nature*, 1990, **347**, 354.
29. M. S. Dresselhaus, G. Dresselhaus, and P.C. Eklund, *J. Raman. Spectrosc.*, 1996, **27**, 351.
30. R. C. Zeller and R. O. Pohl, *Phys. Rev. B.,* 1971*,* **4**, 2029.
31. C. Lee and X. Gonze*, Phys. Rev. B*, 1995, **51**, 8610.
32. A. Einstein, *Ann. Phys.*, 1911, **35**, 679.

33. D. G. Cahill, P. V. Braun, G. Chen, D. R. Clarke, S. Fan, K. E. Goodson, P. Keblinski, W. P. King, G. D. Mahan, A. Majumdar, H. J. Maris, S. R. Phillpot, E. Pop, and L. Shi, *Appl. Phys. Rev.*, 2014, **1**, 011305.
34. M. Born and T. V. Kármán, *Physik Z.*, 1912, **13**, 297.
35. D. T. Morelli, J. P. Heremans, and G. A. Slack, Phys. Rev. B. 2002, **66**, 195304.
36. C. Kittel, *Introduction to Solid State Physics* (8th edition, John Wiley and Sons Inc., New York, USA, 2005).
37. H. J. Goldsmid and A. W. Penn, *Phys. Lett*., 1968, **27A**, 523.